Published in final edited form as:
Epilepsia. 2013 October ; 54(10): . doi:10.1111/epi.12353.

Microstructural Integrity of Early- vs. Late-Myelinating White Matter Tracts in Medial Temporal Lobe Epilepsy

Chu-Yu Lee, PhD[1,2], **Ali Tabesh, PhD**[1,2], **Andreana Benitez, PhD**[1,2], **Joseph A Helpern, PhD**[1,2], **Jens H Jensen, PhD**[1,2], and **Leonardo Bonilha, MD PhD**[2,3]

[1]Department of Radiology and Radiological Science, Medical University of South Carolina, Charleston, SC, USA

[2]Center for Biomedical Imaging, Medical University of South Carolina, Charleston, SC, USA

[3]Comprehensive Epilepsy Center, Division of Neurology, Department of Neurosciences, Medical University of South Carolina, Charleston, SC, USA

Abstract

Purpose—Patients with medial temporal lobe epilepsy (MTLE) exhibit structural brain damage involving gray (GM) and white matter (WM). The mechanisms underlying tissue loss in MTLE are unclear and may be associated with a combination of seizure excitotoxicity and WM vulnerability. The goal of this study was to investigate whether late-myelinating WM tracts are more vulnerable to injury in MTLE compared with early-myelinating tracts.

Methods—Diffusional kurtosis imaging scans were obtained from 25 patients with MTLE and from 36 matched healthy controls. Diffusion measures from regions of interest (ROIs) for both late- and early-myelinating WM tracts were analyzed. Regional Z-scores were computed with respect to normal controls to compare WM in early-myelinating tracts versus late-myelinating tracts.

Key Findings—We observed that late-myelinating tracts exhibited a larger decrease in mean, axial and radial kurtosis compared with early-myelinating tracts. We also observed that the change in radial kurtosis was more pronounced in late-myelinating tracts ipsilateral to the side of seizure onset.

Significance—These results suggest a developmentally based preferential susceptibility of late-myelinating WM tracts to damage in MTLE. Brain injury in epilepsy may be due to the pathological effects of seizures in combination with regional WM vulnerability.

Keywords

Temporal lobe epilepsy; white matter tracts; diffusion tensor imaging; diffusion kurtosis imaging; MRI

Address correspondence to: Leonardo Bonilha MD PhD, 96 Jonathan Lucas St, 3rd floor CSB, Division of Neurology, Department of Neurosciences, Medical University of South Carolina, Charleston, SC 29425, USA, bonilha@musc.edu.

Disclosure of Conflicts of Interest

The authors report no financial or nonfinancial conflicts of interest associated with this study. We confirmed that we have read the Journal's position on issues involved in ethical publication and affirm that this report is consistent with those guidelines.

Introduction

Medial temporal lobe epilepsy (MTLE) is the most common form of epilepsy. MTLE is defined by spontaneous seizures originating from the medial temporal lobe (Engel et al., 1975) and the majority of patients with MTLE demonstrate histological abnormalities in the hippocampus that are collectively termed hippocampal sclerosis (Babb et al., 1984). Hippocampal sclerosis represents cell loss and gliosis within the hippocampus and these abnormalities lead to changes that are often noticeable by qualitative inspection of routine clinical magnetic resonance imaging (MRI) scans. Typically, patients with MTLE demonstrate hippocampal atrophy on T1-weighted images, with concurrent increased hippocampal T2 signal (Cendes et al., 1993; Jack et al., 1990).

Structural abnormalities in MTLE, however, are not restricted to the hippocampus. Other anatomically and functionally connected structures may also exhibit quantifiable changes in MRI, particularly within extra-hippocampal and extra-temporal limbic regions (Bonilha et al., 2003; Gonçalves Pereira et al., 2005; McDonald et al., 2008). Extra-hippocampal structural damage in MTLE is usually more pronounced if the structure is anatomically or functionally closer to the hippocampus. This pattern of damage extending from the medial temporal region suggests the existence of a pathological network mechanism in MTLE evolving from the seizure onset zone and extending into areas of seizure propagation (Bernasconi et al., 2004; Bonilha et al., 2010). The presence of a pathological network in MTLE was first suggested based on findings from manual and voxel-based morphometric studies (Bonilha et al., 2003; Gonçalves Pereira et al., 2005; McDonald et al., 2008). Further studies employing diffusion tensor imaging (DTI) (Basser et al., 1994) also demonstrated an increase in mean diffusivity (MD) and a decrease in the fractional anisotropy (FA) within the limbic system of patients with MTLE (Arfanakis et al., 2002; Concha et al., 2009; Focke et al., 2008; Gross et al., 2006; Thivard et al., 2005), suggesting that white matter (WM) damage follows a network pattern and constitutes an integral component of the pathophysiology of MTLE.

Nonetheless, the mechanisms underlying progressive and extensive structural brain damage seen in MTLE are still unclear. Postulated mechanisms include the excitotoxic effects from seizure activity (Bonilha et al., 2006; Coan et al., 2009; Govindan et al., 2008; Lin et al., 2008), or deafferentation from medial temporal cell loss, but the relationship between these factors is not well established (Arfanakis et al., 2002; Gross et al., 2006; Thivard et al., 2005). Moreover, it is not clear why some WM tracts are more adversely affected than others. For example, excitotoxicity possibly affects regions where seizures initially spread from the seizure onset zone. Nonetheless, more severe microstructural damage has been reported in more distant WM tracts than those that are directly connected to the medial temporal lobe (Otte et al., 2012). Hence, it is likely that WM vulnerability also plays an important role in shaping brain damage in MTLE.

The chronology of myelination during brain development has been recently proposed as an important determinant of WM vulnerability to neurological diseases (Reisberg et al., 1999). Myelination occurs during different developmental epochs in childhood and young adulthood, and the term retrogenesis (Reisberg et al., 1999) describes the relation between developmental myelination and the neurodegenerative process. Originally described in the context of Alzheimer's disease (AD), WM tracts that myelinate late during brain development are postulated to be relatively more vulnerable to the pathological mechanisms from AD compared to the WM tracts that myelinate early. This hypothesis has been corroborated in further imaging studies in AD (Choi et al., 2005; Stricker et al., 2009) and normal aging (Brickman et al., 2012).

In this study, we investigate whether retrogenesis plays a role in the WM damage observed in MTLE. Specifically, we compare the degree of WM damage in early-myelinating tracts versus late-myelinating tracts in patients with MTLE. We assess the microstructural integrity of WM tracts using multiple metrics obtained from diffusion MRI (dMRI) by employing a recently developed extension of DTI termed diffusional kurtosis imaging (DKI) (Jensen et al., 2005). DKI is an extension of conventional DTI, which utilizes multiple diffusion weightings (b-value) to quantify the non-monoexponential decay in diffusion data. DKI is sensitive to changes in non-Gaussian components of water diffusion, and may provide added information regarding the complex mechanisms underlying damage in epilepsy. We hypothesized that late-myelinating WM would exhibit a higher susceptibility to damage in MTLE compared with early-myelinating WM, suggesting that WM loss in MTLE is due to a combination of the pathological mechanisms of epilepsy and inherent WM vulnerability.

Methods

Subjects

Twenty-five consecutive patients (age: 38.6 ± 14.3 years, 15 females) diagnosed with MTLE and thirty-six healthy controls (age: 38.0 ± 11.7 years, 23 females) with no previous neurological or psychiatric history were included in this study. MTLE was diagnosed according to the criteria defined by the International League Against Epilepsy. All patients underwent a comprehensive neurological evaluation and seizures were lateralized according to medical history, neurological examination, interictal electroencephalography (EEG), and prolonged video EEG monitoring with recordings of seizure onset. Ten patients had right MTLE and fifteen patients had left MTLE. The patient and control groups were similar in age and gender distributions. For each patient we collected clinical information regarding age of onset of epilepsy, frequency of seizures, duration of epilepsy and lifetime seizure burden (i.e., the frequency of seizures multiplied by epilepsy duration). None of the patients had a history of status epilepticus. The Institutional Review Board of the Medical University of South Carolina approved this study.

Image acquisition

Image acquisition was performed on a Verio 3 Tesla MR scanner (Siemens Medical, Erlangen, Germany). Diffusion-weighted images (DWIs) were acquired from each patient using a twice-refocused, single-shot echo planar sequence with diffusion weighting applied respectively along 30 non-collinear directions. Images were collected with three b-values: b = 0, 1000, and 2000 s/mm^2. Other imaging parameters were: repetition time = 8500 ms, echo time = 98 ms, field of view = 222 × 222 mm^2, matrix size = 74 × 74, bandwidth: 1324 Hz/pixel, parallel imaging factor of 2, no partial Fourier encoding, number of excitations: 10 for b = 0 s/mm^2, and 1 for b = 1000, 2000 s/mm^2, slice thickness = 3 mm, and 40 axial slices.

Image processing

Image post-processing was carried out using in-house software Diffusional Kurtosis Estimator (Tabesh et al., 2011), which performed the following processing steps to generate voxelwise diffusivity and kurtosis maps. First, motion correction was performed with a six-parameter rigid-body transformation to spatially align all DWIs. Second, at each voxel, the diffusion and diffusional kurtosis tensors were jointly fitted to the DWIs for b = 0, 1000, and 2000 s/mm^2 for that voxel. Finally, FA, MD, axial, and radial diffusivity ($D_{\parallel}$ and $D_{\perp}$), were calculated from the diffusion tensor for the voxel, and mean, axial, and radial kurtoses (MK, $K_{\parallel}$ and $K_{\perp}$) were calculated from the diffusion and kurtosis tensors (Tabesh et al., 2011).

In general, DKI is an extension of DTI since it incorporates an additional term: kurtosis, which is a statistical measure of non-Gaussian diffusion. DKI data is obtained through specific data acquisition parameters, combined with post processing techniques. DKI data is acquired in a similar fashion compared with conventional DTI, but it requires multiple b-values up to 2000 s/mm^2, higher than the b-value = 1000 s/mm^2 typically used in conventional DTI. The multiple b-values are used to quantify the non-Gaussian diffusion, which is demonstrated as non-monoexponential decay in the diffusion data. The non-Gaussian diffusion metric (kurtosis) can be theoretically linked to restricted diffusion and diffusional heterogeneity (Jensen et al., 2005) and may provide extra information about tissue compartments and microstructural heterogeneity, compared with conventional DTI metrics. It is important to notice that reduced diffusional kurtosis indicates a reduction in diffusion heterogeneity (Jensen et al., 2005). Conversely, Increased MK can arise from restricted diffusion, which is associated with reduced MD. Nonetheless, increased diffusion heterogeneity results in higher MK, but MD may not necessarily change if the diffusion magnitude remains unaltered. The original paper on DKI (Jensen et al., 2005) demonstrated that the measured MD and MK in the human brain are weakly correlated.

Image analysis

The FA map for each subject was spatially normalized to the Montreal Neurological Institute (MNI) standard brain using the FMRIB Software Library (FSL) (Smith et al., 2004) and the resulting transformation was applied to the other parametric maps. Figure 1 illustrates all dMRI metrics used in the study (MD, $D_{\parallel}$, $D_{\perp}$, FA, MK, $K_{\parallel}$, $K_{\perp}$) normalized to the MNI standard space. MK is generally higher in WM than in GM, corresponding to a larger degree of microstructural complexity in WM (Jensen & Helpern, 2010; Jensen et al., 2005).

To study the effect of MTLE on the early- and late-myelinating fiber tracts, regions of interest (ROIs) were selected based on the JHU ICBM-DTI-81 WM tractography atlas (Mori et al., 2008). The selection of early- versus late-myelinating tracts was based on previous literature addressing retrogenesis in neurodegenerative disease (Brickman et al., 2012; Choi et al., 2005; Stricker et al., 2009). We aimed to select WM fibers with no direct theoretical involvement in the basic pathophysiology of the MTLE. In MTLE, tracts with a close functional and anatomical relationship with the limbic system are likely to be directly affected during epileptogenesis. Hence, similar to previous studies in degenerative diseases and Alzheimer's disease, where the medial temporal lobe is the initial site of pathogenesis (Brickman et al., 2012), we avoided tracts representing direct input to or outflow from the medial temporal lobe, such as the cingulate fasciculus, fornix and uncinate fasciculus. Early-myelinating fiber tracts included the posterior limb of the internal capsule (PLIC) and the cerebral peduncles (CP). The late-myelinating fiber tracts included the superior longitudinal fasciculus (SLF) and the inferior longitudinal fasciculus (ILF). The selected ROIs for early- and late-myelinating fiber tracts are illustrated in Fig. 2.

Statistical analysis

We evaluated differences between patients and controls for all measures and ROIs with independent sample t-tests (two-tailed, unequal variances assumed) comparing the average dMRI metrics within the ROIs. In total, 28 t-tests were performed (4 ROIs × 7 dMRI metrics), yielding a Bonferroni p corrected for multiple comparisons of $p = 0.0018$, which was used as the threshold for statistical significance. Effect sizes were calculated employing the Cohen's d effect size measure.

To investigate whether late-myelinating tracts exhibited more pronounced damage compared with early-myelinating tracts, we first computed the Z score for each ROI for all patients

(i.e., for each patient, an ROI Z score was computed for each dMRI metric as the number of standard deviations from the mean of controls for that metric). Second, the Z scores from late- (SLF and ILF) and early-myelinating (PLIC and CP) ROIs were each averaged, yielding a combined late-myelinating Z score and a combined early-myelinating Z score. Third, a repeated measures analysis of variance (ANOVA) was performed with one factor representing the chronology of myelination (early versus late). Fourth, we investigated the potential interaction between the chronology of myelination and whether the ROI was ipsilateral or contralateral to the side of seizure onset. This was accomplished with a 2 × 2 repeated measures ANOVA with two factors: side (contralateral versus ipsilateral to seizure onset) and chronology of myelination (early versus late). The p value for statistical significance was set at $p = 0.05$.

We also evaluated the relationship between clinical variables (frequency of seizures, duration of epilepsy and seizure burden) and microstructural data through multiple correlation analyses. The level of significance was set at p = 0.05 corrected for multiple comparisons through False Discovery Rate (Genovese et al., 2002).

Results

Compared with normal controls, patients with MTLE showed a significant decrease in FA, MK and $K_{\perp}$ (Table 1). Particularly, group differences in MK and $K_{\perp}$ metrics were larger in late-myelinating tracts (SLF and ILF) compared with the differences in early-myelinating tracts (PLIC and CP). Significantly lower MK and $K_{\perp}$ were observed in both SLF and ILF, but only lower $K_{\perp}$ were observed in CP. In addition, the Cohen's d effect sizes of MK and $K_{\perp}$ were larger in SLF and ILF than in CP.

Kurtosis metrics were more sensitive to group differences in late-myelinating tracts than FA (Table 1). This was demonstrated by the larger Cohen's d effect sizes of MK and $K_{\perp}$ in SLF and ILF compared to the effect sizes of FA.

Significantly lower Z scores were observed for MK, $K_{\parallel}$ and $K_{\perp}$ for late-myelinating ROIs, irrespective of the side of ROIs (Fig. 3).

A significant interaction was also noted between the chronology of myelination and side of the WM tracts (Fig. 4), and was only observed with $K_{\perp}$ metrics. The interaction indicates that reductions of $K_{\perp}$ were more pronounced in late-myelinating tracts ipsilateral to the side of seizure onset.

We did not observe a significant correlation between clinical variables and microstructural measures obtained from dMRI.

Discussion

In this study, we investigated whether the chronology of myelination is associated with WM vulnerability in MTLE. Specifically, we assessed whether WM tracts known to myelinate late in life exhibited more pronounced damage compared with WM tracts known to myelinate early in life.

Using dMRI metrics sensitive to tissue microstructure, we observed that late-myelinating tracts exhibited a higher degree of damage in comparison to early-myelinating tracts. Specifically, a significant reduction in MK, $K_{\parallel}$ and $K_{\perp}$ was observed in late myelinating tracts in patients with MTLE compared to controls (Table 1 and Fig. 3). Finally, we observed a significant interaction between side of seizure onset and chronology of

myelination (Fig. 4) since WM tracts ipsilateral to the side of seizure onset demonstrated a more pronounced degree of damage.

Our results suggest that the chronology of myelination may be a contributing factor underlying WM damage in MTLE, a phenomenon that has been observed in AD and normal aging (Choi et al., 2005; Stricker et al., 2009; Brickman et al., 2012). Chronology of myelination is also likely not the single determinant of WM injury in MTLE and other important pathological mechanisms may play a role in cell loss in MTLE, particularly seizure excitotoxicity and deafferentation (Bonilha et al., 2010; Concha et al., 2012).

The multifactorial nature of WM damage in MTLE is corroborated by our observation regarding the significant interaction between chronology of myelination and lateralization of the seizure onset zone. The presence of more pronounced changes in dMRI metrics ipsilateral to seizure onset suggest that damage can ensue from proximity to the area of initial seizure onset and propagation, or deafferentation from anatomical connections to the more affected hippocampus and medial temporal lobe. Importantly, these features may interact with the chronology of myelination to account for the resulting damage.

A potential confounder in this study is the closer functional relationship between late-myelinating tracts and the medial temporal lobe. While early myelinating tracts represent primary somatosensory functions (i.e., primary brain outflow and input), late myelinating fibers represent cortical-cortical connections. The late-myelinating tracts evaluated in this study (ILF and SLF) correspond to connections involving secondary and tertiary brain regions. It is not possible to determine if cortical-cortical networks are initially affected by seizures and epileptogenesis compared with somatosensory regions. We avoided tracts corresponding to direct input or outflow from the medial temporal lobe, but the possibility that seizures initially affect late myelinating tracts cannot be excluded by this study. It is also noteworthy that the SLF exhibited significant damage in spite of its relative anatomical distance to the medial temporal lobe. Furthermore, there is likely a multi-step relationship composed of ontogenesis leading to functional organization leading in turn to excitotoxicity. It is not possible to determine whether damage is a direct consequence of ontogenesis or a consequence of the functional organization resulting from ontogenesis.

Interestingly, WM damage in general, and specifically WM damage involving late-myelinating tracts, was more strongly observed with kurtosis metrics. As summarized in Table 1, FA was reduced on both early and late myelinating tracts, while MK was reduced only on late myelinating tracts, and radial kurtosis was reduced on early and late myelinating tracts. It is noteworthy that the effect size was larger on late myelinating tracts when employing DKI measures, but larger on early myelinating tracts with FA measures. These findings suggest that FA and diffusional kurtosis measures are sensitive to different phenomena. Kurtosis is a statistical measure of non-Gaussian diffusion, while FA is a measure of anisotropy of diffusivity. Thus, kurtosis may provide additional information about microstructural changes instead of replacing DTI metrics, e.g. FA. FA changes in MTLE may reflect a possible increase in the degree of gliosis and myelin degradation, whereas kurtosis alternations may be associated with a combination of axonal loss and permeability changes between the intra- and extra-axonal compartments. Through tissue modeling, kurtosis parameters have been specifically linked to the tissue properties of intra- and extra-axonal compartments, including axonal water fraction, axonal diffusivity, and extra-axonal tortuosity (Fieremans et al., 2011). We postulate that MTLE is associated with complex pathological mechanisms involving neuronal loss, replacement of neurons by glial cells, compromised axonal membrane and myelin integrity (Concha et al., 2010). These processes involve complex changes in heterogeneous tissue compartments that may not be reflected by bulk diffusivity measured by conventional DTI metrics but are better

characterized by kurtosis measures. The larger effect observed with $K_{\perp}$ suggests that reduction in longitudinal diffusion with preservation of membrane compartmentalization may be an important component of the changes observed. These phenomena are relevant in the context of pathogenesis of epilepsy and should be explored by future studies.

It is also noteworthy that laterality of damage was demonstrated with $K_{\perp}$ but not with other modalities. For example, FA demonstrated significant damage on both hemispheres, but there was not an interaction between time of myelination and laterality. It is also noteworthy that we did not observe more prominent asymmetries. Nonetheless, asymmetrical WM damage is usually more pronounced in regions underlying the medial temporal lobe (Bonilha et al., 2010; Focke et al., 2008), which were purposefully avoided for this study. It is possible that the mechanisms leading to WM damage in epilepsy are the results of a complex interaction between ontogenesis, seizure excitotoxicity and the proximity of the WM pathways to the networks underlying seizure onset. Importantly, WM damage in epilepsy is not a homogenous process, and pathological processes may weigh differently depending on the anatomical and functional properties of the WM tracts. Likewise, the absence of significant correlations between clinical variables and imaging data could reflect the lack of statistical power to detect such as relationship, or that most of the damage may occur during key steps in epileptogenesis, and may not be related to the overall seizure burden. This may also be explored by future studies.

In conclusion, we used dMRI to study the microstructural integrity of early- and late-myelinating WM tracts in MTLE. We demonstrated that late-myelinating WM tracts are more sensitive to MTLE-related microstructural damage compared with early-myelinating WM tracts, suggesting that the chronology of myelination may be a factor involved in microstructural damage due to seizures. Furthermore, we demonstrated that kurtosis metrics derived from DKI are particularly sensitive to microstructural tissue damage in MTLE. These results may be useful in better understanding the pathologic mechanisms of epilepsy.

Acknowledgments

This work was supported in part by South Carolina Clinical & Translational Research Institute through NIH Grant Numbers UL1 RR029882 and UL1 TR000062.

References

Arfanakis K, Hermann BP, Rogers BP, Carew JD, Seidenberg M, Meyerand ME. Diffusion tensor MRI in temporal lobe epilepsy. Magn Reson Imaging. 2002; 20:511–519. [PubMed: 12413596]

Babb TL, Brown WJ, Pretorius J, Davenport C, Lieb JP, Crandall PH. Temporal lobe volumetric cell densities in temporal lobe epilepsy. Epilepsia. 1984; 25:729–740. [PubMed: 6510381]

Basser PJ, Mattiello J, LeBihan D. Estimation of the effective self-diffusion tensor from the NMR spin echo. J Magn Reson B. 1994; 103:247–254. [PubMed: 8019776]

Bernasconi N, Duchesne S, Janke A, Lerch J, Collins DL, Bernasconi A. Whole-brain voxel-based statistical analysis of gray matter and white matter in temporal lobe epilepsy. NeuroImage. 2004; 23:717–723. [PubMed: 15488421]

Bonilha L, Kobayashi E, Rorden C, Cendes F, Li LM. Medial temporal lobe atrophy in patients with refractory temporal lobe epilepsy. J Neurol Neurosurg Psychiatry. 2003; 74:1627–1630. [PubMed: 14638879]

Bonilha L, Rorden C, Appenzeller S, Coan AC, Cendes F, Li LM. Gray matter atrophy associated with duration of temporal lobe epilepsy. NeuroImage. 2006; 32:1070–1079. [PubMed: 16872843]

Bonilha L, Edwards JC, Kinsman SL, Morgan PS, Fridriksson J, Rorden C, Rumboldt Z, Roberts DR, Eckert MA, Halford JJ. Extrahippocampal gray matter loss and hippocampal deafferentation in patients with temporal lobe epilepsy. Epilepsia. 2010; 51:519–528. [PubMed: 20163442]

Brickman A, Meier I, Korgaonkar M, Provenzano F, Grieve S, Siedlecki K, Wasserman B, Williams L, Zimmerman M. Testing the white matter retrogenesis hypothesis of cognitive aging. Neurobiol Aging. 2012; 33:1699–1715. [PubMed: 21783280]

Cendes F, Andermann F, Gloor P, Evans A, Jones-Gotman M, Watson C, Melanson D, Olivier A, Peters T, Lopes-Cendes I. MRI volumetric measurement of amygdala and hippocampus in temporal lobe epilepsy. Neurology. 1993; 43:719–725. [PubMed: 8469329]

Choi SJ, Lim KO, Monteiro I, Reisberg B. Diffusion tensor imaging of frontal white matter microstructure in early Alzheimer's disease: a preliminary study. J Neurol Neurosurg Psychiatry. 2005; 18:12–19.

Coan AC, Appenzeller S, Bonilha L, Li LM, Cendes F. Seizure frequency and lateralization affect progression of atrophy in temporal lobe epilepsy. Neurology. 2009; 73:834–842. [PubMed: 19752449]

Concha L, Beaulieu C, Collins DL, Gross DW. White-matter diffusion abnormalities in temporal-lobe epilepsy with and without mesial temporal sclerosis. J Neurol Neurosurg Psychiatry. 2009; 80:312–319. [PubMed: 18977826]

Concha L, Livy DJ, Beaulieu C, Wheatley BM, Gross DW. In vivo diffusion tensor imaging and histopathology of the fimbria-fornix in temporal lobe epilepsy. J Neurosci. 2010; 30:996–1002. [PubMed: 20089908]

Concha L, Kim H, Bernasconi A, Bernhardt BC, Bernasconi N. Spatial patterns of water diffusion along white matter tracts in temporal lobe epilepsy. Neurology. 2012; 79:455–462. [PubMed: 22815555]

Engel J Jr, Driver MV, Falconer MA. Electrophysiological correlates of pathology and surgical results in temporal lobe epilepsy. Brain. 1975; 98:129–156. [PubMed: 1122371]

Fieremans E, Jensen JH, Helpern JA. White matter characterization with diffusional kurtosis imaging. NeuroImage. 2011; 58:177–188. [PubMed: 21699989]

Focke NK, Yogarajah M, Bonelli SB, Bartlett PA, Symms MR, Duncan JS. Voxel-based diffusion tensor imaging in patients with mesial temporal lobe epilepsy and hippocampal sclerosis. NeuroImage. 2008; 40:728–737. [PubMed: 18261930]

Genovese CR, Lazar NA, Nichols T. Thresholding of statistical maps in functional neuroimaging using the false discovery rate. Neuroimage. 2002; 15:870–878. [PubMed: 11906227]

Gonçalves Pereira PM, Insausti R, Artacho-Pérula E, Salmenperä T, Kälviäinen R, Pitkänen A. MR volumetric analysis of the piriform cortex and cortical amygdala in drug-refractory temporal lobe epilepsy. AJNR Am J Neuroradiol. 2005; 26:319–332. [PubMed: 15709130]

Govindan RM, Makki MI, Sundaram SK, Juhász C, Chugani HT. Diffusion tensor analysis of temporal and extra-temporal lobe tracts in temporal lobe epilepsy. Epilepsy research. 2008; 80:30–41. [PubMed: 18436432]

Gross DW, Concha L, Beaulieu C. Extratemporal white matter abnormalities in mesial temporal lobe epilepsy demonstrated with diffusion tensor imaging. Epilepsia. 2006; 47:1360–1363. [PubMed: 16922882]

Jack CR, Sharbrough FW, Twomey CK, Cascino GD, Hirschorn KA, Marsh WR, Zinsmeister AR, Scheithauer B. Temporal lobe seizures: lateralization with MR volume measurements of the hippocampal formation. Radiology. 1990; 175:423–429. [PubMed: 2183282]

Jensen JH, Helpern JA, Ramani A, Lu H, Kaczynski K. Diffusional kurtosis imaging: the quantification of non-gaussian water diffusion by means of magnetic resonance imaging. Magn Reson Med. 2005; 53:1432–1440. [PubMed: 15906300]

Jensen JH, Helpern JA. MRI quantification of non-Gaussian water diffusion by kurtosis analysis. NMR Biomed. 2010; 23:698–710. [PubMed: 20632416]

Lin JJ, Riley JD, Juranek J, Cramer SC. Vulnerability of the frontal-temporal connections in temporal lobe epilepsy. Epilepsy Res. 2008; 82:162–170. [PubMed: 18829258]

McDonald CR, Hagler DJ Jr, Ahmadi ME, Tecoma E, Iragui V, Gharapetian L, Dale AM, Halgren E. Regional neocortical thinning in mesial temporal lobe epilepsy. Epilepsia. 2008; 49:794–803. [PubMed: 18266751]

Mori S, Oishi K, Jiang H, Jiang L, Li X, Akhter K, Hua K, Faria AV, Mahmood A, Woods R, Toga AW, Pike GB, Neto PR, Evans A, Zhang J, Huang H, Miller MI, van Zijl P, Mazziotta J.

Stereotaxic white matter atlas based on diffusion tensor imaging in an ICBM template. NeuroImage. 2008; 40:570–582. [PubMed: 18255316]

Moseley ME, Cohen Y, Kucharczyk J, Mintorovitch J, Asgari HS, Wendland MF, Tsuruda J, Norman D. Diffusion-weighted MR imaging of anisotropic water diffusion in cat central nervous system. Radiology. 1990; 176:439–445. [PubMed: 2367658]

Otte WW, van Eijsden P, Sander JW, Duncan JS, Dijkhuizen RM, Braun KP. A meta-analysis of white matter changes in temporal lobe epilepsy as studied with diffusion tensor imaging. Epilepsia. 2012; 53:659–667. [PubMed: 22379949]

Reisberg B, Franssen EH, Hasan SM, Monteiro I, Boksay I, Souren LE, Kenowsky S, Auer SR, Elahi S, Kluger A. Retrogenesis: clinical, physiologic, and pathologic mechanisms in brain aging, Alzheimer's and other dementing processes. Eur Arch Psychiatry Clin Neurosci. 1999; 249(Suppl 3):28–36. [PubMed: 10654097]

Smith S, Jenkinson M, Woolrich M, Beckmann C, Behrens T, Johansen-Berg H, Bannister P, De Luca M, Drobnjak I, Flitney D, Niazy R, Saunders J, Vickers J, Zhang Y, De Stefano N, Brady M, Matthews P. Advances in functional and structural MR image analysis and implementation as FSL. NeuroImage. 2004; 23(Suppl 1):S208–S219. [PubMed: 15501092]

Stricker NH, Schweinsburg BC, Delano-Wood L, Wierenga CE, Bangen KJ, Haaland KY, Frank LR, Salmon DP, Bondi MW. Decreased white matter integrity in late-myelinating fiber pathways in Alzheimer's disease supports retrogenesis. NeuroImage. 2009; 45:10–16. [PubMed: 19100839]

Tabesh A, Jensen JH, Ardekani BA, Helpern JA. Estimation of tensors and tensor-derived measures in diffusional kurtosis imaging. Magn Reson Med. 2011; 65:823–836. [PubMed: 21337412]

Thivard L, Lehéricy S, Krainik A, Adam C, Dormont D, Chiras J, Baulac M, Dupont S. Diffusion tensor imaging in medial temporal lobe epilepsy with hippocampal sclerosis. NeuroImage. 2005; 28:682–690. [PubMed: 16084113]

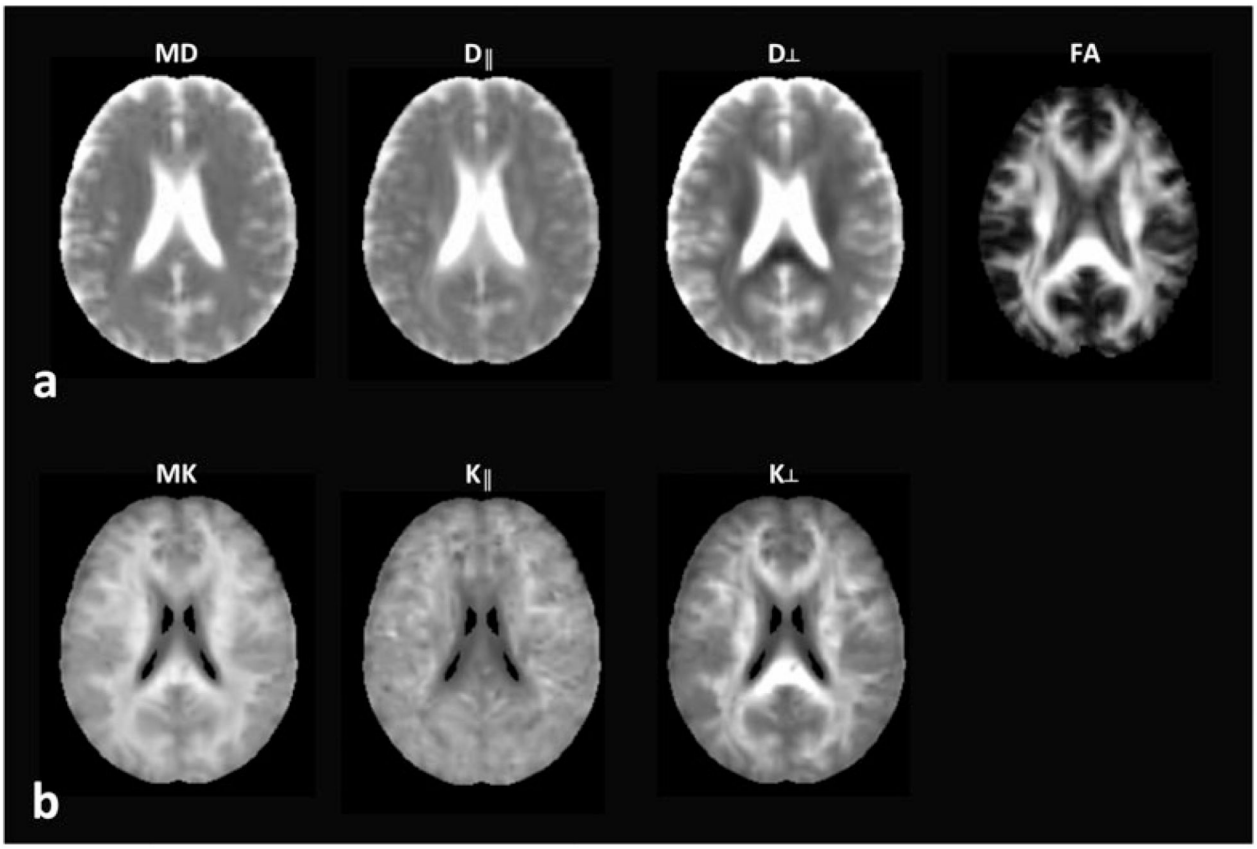

Figure 1.
An example of spatially normalized parametric maps derived from dMRI: mean diffusivity (MD), axial diffusivity ($D_{\parallel}$), radial diffusivity ($D_{\perp}$), fractional anisotropy (FA), mean kurtosis (MK), axial kurtosis ($K_{\parallel}$), and radial kurtosis ($K_{\perp}$).

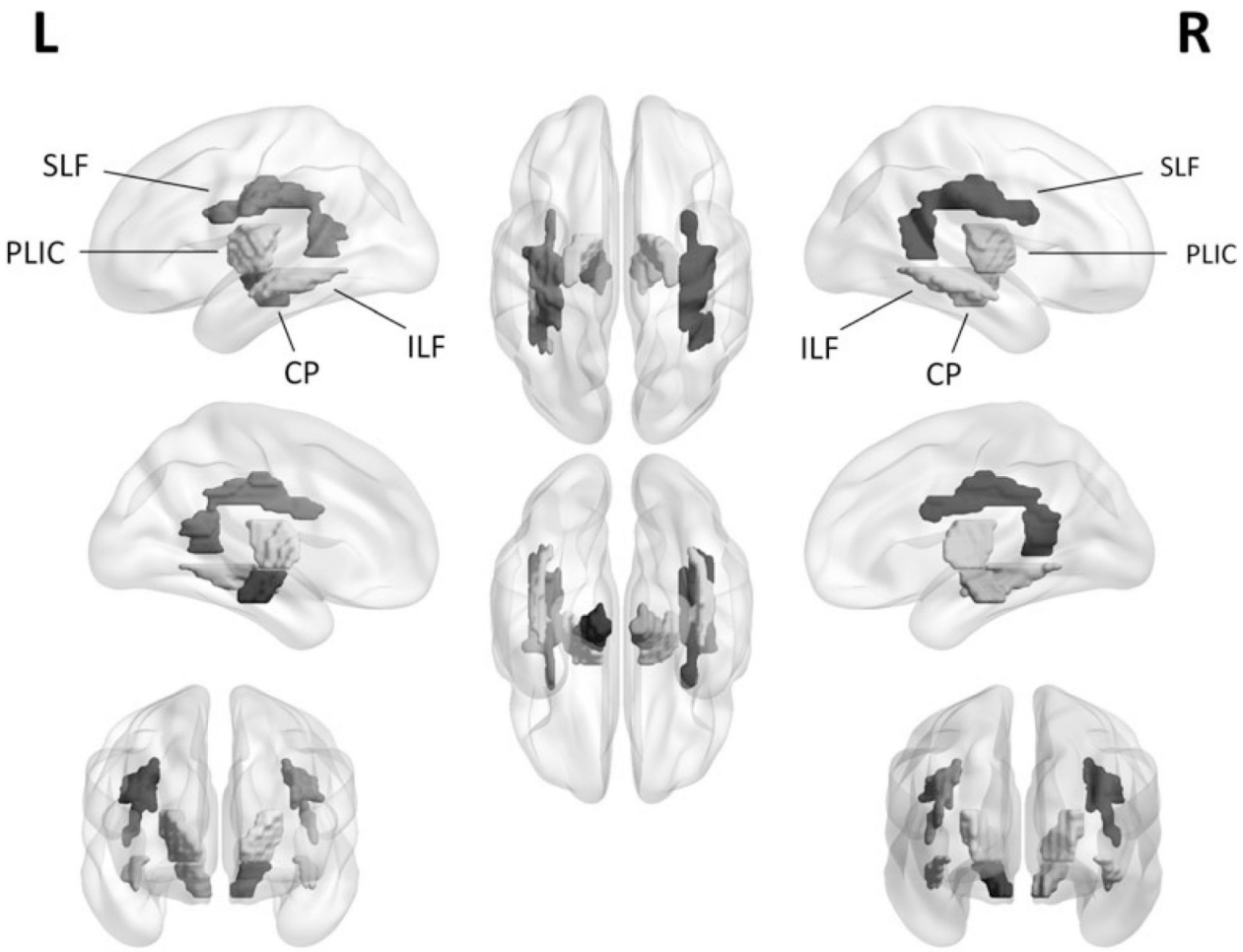

Figure 2.
Three-dimensional representation of selected ROIs for early-myelinating fiber tracts: posterior limb of the internal capsule (PLIC) and cerebral peduncles (CP), and for late-myelinating fiber tracts: superior longitudinal fasciculus (SLF) and inferior longitudinal fasciculus (ILF).

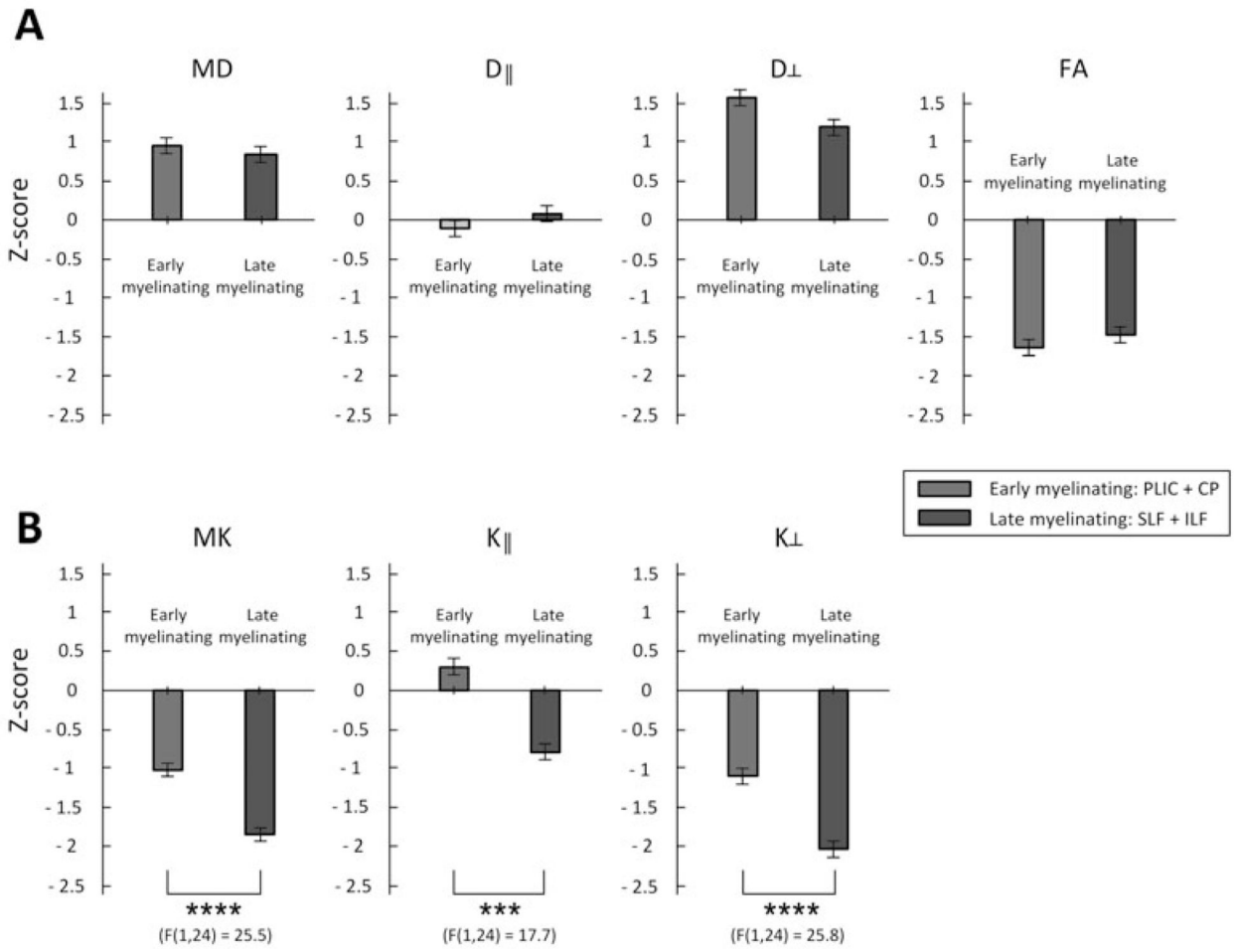

Figure 3.

Comparisons of Z-scores (deviation from the mean of normal controls) in the early- and late-myelinating fiber tracts of the MTLE group; *: $p < 0.05$, **: $p < 0.01$, ***: $p < 0.001$, ****: $p < 0.0001$, evaluated with a repeated measure ANOVA (one factor). Error bars represent the standard error.

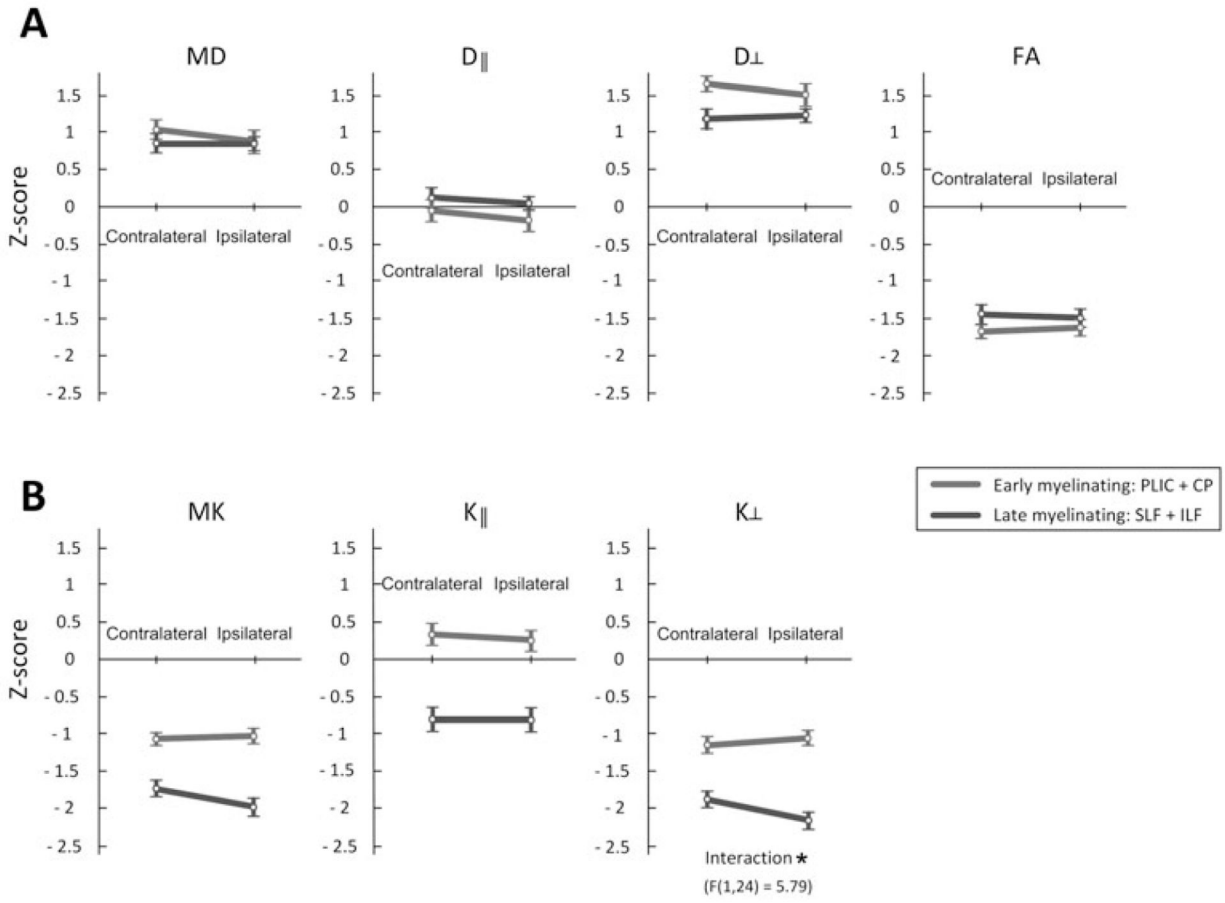

Figure 4.

Z-score differences between contralateral and ipsilateral sides and between early- and late-myelinating fiber tracts of the MTLE group. Differences exhibited a significant interaction: * ($p < 0.05$), evaluated with a repeated measure ANOVA with two factors: side (contralateral versus ipsilateral to seizure onset) and chronology of myelination (early versus late). Error bars represent the standard error.

Table 1

dMRI derived parameters - mean (standard deviation) – from ROIs from normal controls (n = 36) and patients with MTLE (n = 25).

Regions	Controls (n = 36)	MTLE (n = 25)	t-statistic	Cohen's d
MD ($\mu m^2/ms$)				
Early-myelinating				
PLIC	0.80 (0.02)	0.82 (0.07)	1.37	0.41
CP	1.04 (0.05)	1.11 (0.12)	2.75	0.81
Late-myelinating				
SLF	0.84 (0.03)	0.87 (0.05)	2.06	0.75
ILF	1.05 (0.07)	1.11 (0.14)	1.99	0.74
$D_{\parallel}$ ($\mu m^2/ms$)				
Early-myelinating				
PLIC	1.34 (0.04)	1.32 (0.09)	−1.06	−0.20
CP	1.69 (0.06)	1.73 (0.13)	1.33	0.38
Late-myelinating				
SLF	1.22 (0.03)	1.23 (0.06)	0.04	0.13
ILF	1.55 (0.09)	1.58 (0.16)	0.74	0.37
$D_{\perp}$($\mu m^2/ms$)				
Early-myelinating				
PLIC	0.52 (0.02)	0.56 (0.06)	2.96	0.97
CP	0.71 (0.05)	0.80 (0.12)	3.41	0.99
Late-myelinating				
SLF	0.65 (0.03)	0.69 (0.05)	2.92	0.99
ILF	0.80 (0.06)	0.88 (0.14)	2.68	0.93
FA				
Early-myelinating				
PLIC	0.54 (0.02)	0.51 (0.03) **	−4.99	−1.42
CP	0.52 (0.03)	0.48 (0.04) **	−4.50	−1.26
Late-myelinating				
SLF	0.40 (0.02)	0.38 (0.03) *	−4.01	−1.20
ILF	0.42 (0.02)	0.38 (0.03) **	−5.07	−1.46
MK				
Early-myelinating				
PLIC	1.14 (0.07)	1.07 (0.12)	−2.76	−0.79
CP	1.11 (0.06)	1.05 (0.08)	−3.13	−0.88
Late-myelinating				
SLF	1.15 (0.04)	1.07 (0.07) **	−5.14	−1.47
ILF	0.93 (0.04)	0.85 (0.06) ***	−5.32	−1.49
$K_{\parallel}$				
Early-myelinating				

Regions	Controls (n = 36)	MTLE (n = 25)	t-statistic	Cohen's d
PLIC	0.72 (0.03)	0.73 (0.04)	0.73	0.20
CP	0.69 (0.03)	0.70 (0.04)	1.32	0.37
Late-myelinating				
SLF	0.93 (0.03)	0.90 (0.03)	−3.45	−0.92
ILF	0.71 (0.02)	0.69 (0.04)	−1.90	−0.54
$K_{\perp}$				
Early-myelinating				
PLIC	1.58 (0.14)	1.42 (0.24)	−3.07	−0.87
CP	1.58 (0.12)	1.44 (0.16) *	−3.91	−1.07
Late-myelinating				
SLF	1.55 (0.09)	1.36 (0.13) ****	−6.31	−1.76
ILF	1.23 (0.08)	1.07 (0.11) ****	−6.58	−1.81

* $p < 0.0018$ (Bonferroni corrected significance level)

** $p < 10^{-4}$

*** $p < 10^{-5}$

**** $p < 10^{-6}$ with the independent sample t-test (two-tailed, unequal variances assumed).